Contribution to the corrosion inhibition of aluminum in 1 M HCl by *Pimpinella Anisum* extract. Experimental and theoretical studies (DFT, MC, and MD)

Z. Akounach,[1,2] A. Al Maofari,[1,3] M. Damej,[1,2] S. El Hajjaji,[1]* A. Berisha,[4,5] V. Mehmeti,[4,5] N. Labjar,[6] M. Bamaarouf[2] and M. Benmessaoud[2]

[1]*Laboratory of Spectroscopy, Molecular Modelling Materials, Nanomaterials Water and Environment – CERNE2D, Faculty of Sciences, Mohammed V University in Rabat, B.P. 1014 RP Rabat, Morocco*

[2]*Environment, Materials and Sustainable Development Team – CERNE2D, High School of Technology of Salé, Mohammed V University in Rabat, BP 227 Sale, Morocco*

[3]*Laboratory of Physical Chemistry, Faculty of Education, Art and Sciences, Amran University, Yemen*

[4]*Department of Chemistry, Faculty of Natural and Mathematics Science, University of Prishtina, 10000 Prishtina, Kosovo*

[5]*Materials Science – Nanochemistry Research Group, NanoAlb-Unit of Albanian Nanoscience and Nanotechnology, 1000 Tirana, Albania*

[6]*Laboratory of Spectroscopy, Molecular Modelling Materials, Nanomaterials Water and Environment – CERNE2D, ENSAM, Mohammed V University in Rabat, B.P. 1014 RP Rabat, Morocco*

**E-mail: souad.elhajjaji@fsr.um5.ac.ma*

Abstract

Corrosion inhibition of aluminum in 1 M hydrochloric acid solution by aqueous extract of *Pimpinella anisum* was studied using linear polarization, electrochemical impedance spectroscopy (EIS) and Density Functional Theory (DFT). *Pimpinella Anisum* plant was used. The results show an excellent performance of the aqueous extract as a corrosion inhibitor for aluminum. The inhibition efficiency was found to increase with increasing concentration of *Pimpinella Anisum* aqueous extract. The electrochemical measurements showed that the *Pimpinella Anisum* extract acts as a mixed-type inhibitor. The inhibition is due to adsorption of the extract molecules on the aluminum surface according to the Langmuir adsorption isotherm. DFT calculations and MD simulations were used to explain the adsorption mode on the metal surface and to determine the adsorption centers of this inhibitor. DFT, MC, and MD calculations show a strong adsorption interaction between the extract molecules and the metal surface. Scanning electron microscopy (SEM) coupled with energy dispersive spectroscopy (EDS) study confirmed that the corrosion inhibition of aluminum occurs through adsorption of the extract's molecules on the metal surface. The theoretical calculations are in good agreement with the experimental results.

Received: August 16, 2021. Published: March 28, 2022 doi: 10.17675/2305-6894-2022-11-1-24

Keywords: *corrosion inhibition, polarization, adsorption, theoretical study, DFT-MD.*

1. Introduction

Aluminum and its alloys have an exceptional industrial and economic importance due to their exceptional inherent properties such as low density, high strength-to-weight ratio, excellent electrical and thermal conductivity, and high ductility. The most important feature of this metal is its corrosion resistance owing to the formation of a protective film on the surface when it is in contact with a corrosive environment (atmosphere or water) [1–4]. Usually, the film is stable in solutions with pH 4.5–8.5, but it has a high solubility in strong acid and alkaline media, consequently, the metal presents a high rate of corrosion [5].

Generally, hydrochloric acid solutions are used for pickling, industrial cleaning, chemical and electrochemical etching of aluminum, where corrosion is uniform and the dissolution rate is very high. So, it is important to protect aluminum to achieve lower dissolution [2]. Diverse methods are suggested for protection against corrosion in acid media. The most common one is the use of corrosion inhibitors [6]. In the majority of cases, organic molecules containing electronegative atoms such as N, O, S, unsaturated bonds and/or aromatic rings are used [7]. The use of chemical inhibitors stays a good anticorrosive method, as it is most cost-effective, convenient and practical. Unfortunately, these chemical inhibitors are hazardous for health, and for security and safety reasons, the search and development are oriented to use natural products of plant origin (extract of some plant seeds, leaves, stems, fruit) as anti-corrosion agents which are non-toxic, environmentally friendly, and harmless [4, 5, 8–16]. Al-Hosary *et al*. [17] were among the first researches who used natural products of plant origin as corrosion inhibitors. They studied the inhibition of Al and Zn dissolution in HCl and NaOH by aqueous extract of *Hibiscus Sabdariffa*, which was effective to decrease the dissolution of the two metals.

Pimpinella Anisum is an annual herb and a grassy plant with white flowers and small green to yellow seeds that grows in India, Yemen, Morocco, Turkey, and many other warm regions of the world. The extract from the seeds of *Anisum* contains anethole and it is valuable in cosmetic and medicine domains [18–23].

The aim of this work was to study the corrosion inhibition of aluminum in acid solution by aqueous extracts of *Pimpinella Anisum* using potentiostatic polarization, electrochemical impedance spectroscopy techniques, and density functional theory calculations. The state of aluminum surface was examined by scanning electron microscopy coupled to EDX.

2. Materials and Methods

2.1. Plants material

Pimpinella Anisum or aniseed is locally known as “anis vert”, an annual herb belonging to the *Umbelliferae* family, 30–50 cm high, with white flowers and small green to yellow seeds. It is one of the oldest medicinal plants; it grows in the east of the Mediterranean region, the Middle East, and the west of Asia. This plant is mostly grown for its fruits which are

used for flavoring and for various purposes. In traditional medicine, anise seeds are used as an analgesic, disinfectant and to increase milk production. It is also effective in polishing of teeth [24–29]. The aniseed contains volatile oil (1.5–6.0 mass%), lipids (8–11 mass%), carbohydrates (≈ 4 mass%), and proteins (18 mass%) [29].

2.2. Samples preparation and extraction

The grains of *Pimpinella Anisum* were dried in laboratory at room temperature and finally grinded. The extraction was performed by the maceration technique in hot distilled water (60°C) for two hours. An aqueous extract of the grains was prepared and afterward used as a corrosion inhibitor at various concentration in this study.

2.3. Working electrode and corrosive solution

The working electrode had the shape of a disc of the aluminum alloy and embedded in epoxy resin to allow the cross-section of 1 cm^2 to be immersed in the corrosive solution.

The corrosive solution utilized was set up by dissolution of analytical reagent 37% HCl in distilled water.

2.4. Electrochemical measurements

The electrochemical measurements were performed in a conventional electrochemical three electrode cell with a platinum wire as a counter electrode (CE), a saturated calomel electrode (SCE) as a reference electrode (RE), and an aluminum electrode as a working electrode (WE). The working electrode surface was abraded successively with fine grade emery papers (1000, 1200, 2000) and then the metal surface was rinsed with bidistilled water.

For all stationary and transient measurements, a Voltalab 301 PGZ potentiostat controlled by a PC and Voltamaster 4.0 software was used to run the tests, collect, and evaluate the experimental data. The electrode potential was allowed to reach a steady value after 60 min before starting the measurements.

To obtain the polarization curves, the potential was varied from –1200 to –200 mV *versus* SCE at a scanning rate of 1 mV/s. The inhibition efficiency *IE*% was calculated from the following equation (1) [30, 31]:

$$IE\% = \frac{i_{corr}^{0} - i_{corr}}{i_{corr}^{0}} \cdot 100 \quad (1)$$

where i_{corr}^{0} and i_{corr} are the uninhibited and inhibited corrosion current density values, respectively.

To obtain electrochemical impedance curves, the frequency is varied in the range from 100 kHz to 10 mHz. The inhibition efficiency *IE*% was calculated from the following equation (2) [32]:

$$IE\% = \frac{R_{\mathrm{P}}^{-1} - R_{\mathrm{P(inh)}}^{-1}}{R_{\mathrm{P}}^{-1}} \quad (2)$$

where $R_{\mathrm{P(inh)}}$ and R_{P} are the polarization resistance in the presence and in the absence of the inhibitor, respectively.

2.5. Scanning electron microscopy

Scanning Electron Microscope coupled with EDX was used to monitor surface morphological changes. The analysis by SEM/EDX was carried out on the surface of aluminum samples before and after immersion for 24 h in 1 M HCl acid solutions with and without the optimal concentration of 3 g/L of the plant extract. The specimens were cleaned with distilled water and used for the analysis.

2.6. DFT calculation

DFT calculations were finalized using the Dmol^3 software from Biovia [33, 34]. Generalized Gradient Approximation [35, 36] employing the M06-L [37–39] and the Double Numeric quality basis set (DNP) [40] were used for geometry optimizations. Self-consistent-field (SCF) convergence norm was set to be smaller than $1 \cdot 10^{-6}$ eV. The energy minima were proven by doing a vibrational analysis and confirming the absence of any imaginary frequencies [41].

2.7. Monte Carlo (MC) and Molecular Dynamic (MD) simulation

The interaction between aluminum surface and anethole, fenchone, limonene and *p*-allylanisole inhibitors was performed in the simulated corrosion milieu by using the 4 atom-thick layer unit cell of Al(111) surface (under Periodic Boundary Condition). The sizes of the slab model were: 20.044 Å×20.044 Å×7.064 Å with an enclosed addition of 30 Å vacuum layer at the *C* axis that was inserted with: 1 inhibitor molecule (anethole, fenchone, limonene or *p*-allylanisole)/350 H_2O molecules/5 chloride + 5 hydronium ions. Beforehand the MD step, the geometry of the simulation boxes was optimized (energy converges with a tolerance of $1 \cdot 10^{-5}$ kcal/mol; the atom-based summation method was applied for both Electrostatic and van der Waals interaction with a cutoff distance of 15.5 Å, a spline width of 1 Å and a 0.5 Å buffer) using the Forcite module fused in the Biovia software package [42, 43, 44].

MD was performed over the canonical constant volume/constant temperature (NVT) ensemble at 25°C [43] with a simulation time of 500 ps (1 fs time step) [45]. The *T* parameter is retained back by the Berendsen thermostat. MC and MD calculations are done using the Condensed Phase Optimized Molecular Potential II (COMPASSII) forcefield [43, 46, 48]. Radial Distribution Function (RDF) analysis is done on the second half of the MD trajectory [32, 49, 50].

3. Results and Discussion

3.1. Chemical composition of Pimpinella Anisum extract

The chemical composition was determined by CPG-MS, the most widespread technique used in the field of essential oils and extracts. In most cases, it makes it possible to find the molecular mass of a compound and to obtain structural information relating to a molecule from its fragmentation.

The chromatogram obtained from the extract of *Pimpinella anisum* is shown in Figure 1.

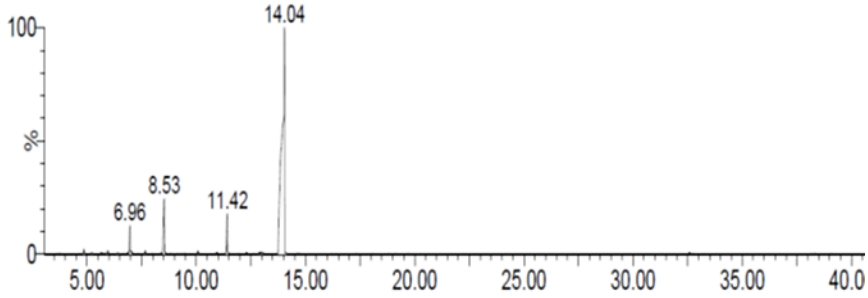

Figure 1. Chromatogram of the *Pimpinella anisum* extract.

Chromatogram of the Anise aqueous extract showed 4 peaks corresponding to 4 major compounds. The allocation of the different peaks is shown in Table 1.

Table 1: Data obtained by CPG-MS of Anise aqueous extract.

Noun	Empirical formula	Structure
Limonene	$C_{10}H_{16}$	
Fenchone	$C_{10}H_{16}O$	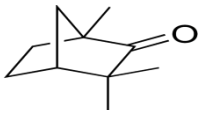
p-Allylanisole	$C_{10}H_{12}O$	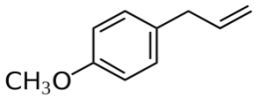
Anethole	$C_{10}H_{12}O$	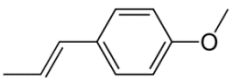

3.2. Electrochemical experiments

3.2.1. Polarization curves

The inhibition of the *Pimpinella Anisum* extract on aluminum samples immersed in 1 M HCl was studied by measuring the modification of the cathodic and anodic behavior of the

samples. Figure 2 shows the anodic and cathodic polarization curves of aluminum in 1 M HCl solution in the absence and in the presence of the *Pimpinella Anisum* extract. The electrochemical parameters: corrosion potential (E_{corr}), corrosion current density (i_{corr}), cathodic and anodic Tafel slopes (β_c and β_a) were calculated from the intersection of the cathodic and anodic Tafel lines at E_{corr}. All the parameters obtained from the polarization measurements are listed in Table 2.

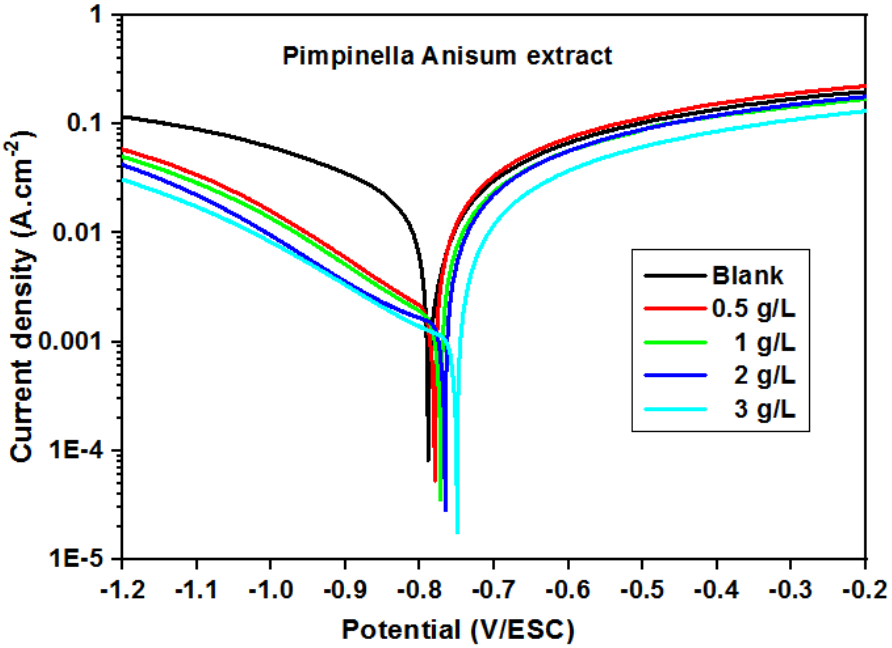

Figure 2. Polarization curves of aluminum in 1 M HCl in the absence and in the presence of *Pimpinella Anisum* extract.

Table 2. Parameters of polarization curves for aluminum corrosion in 1 M HCl solution containing different concentrations of the inhibitor.

Concentration (g/L)	E_{corr} **(mV/SCE)**	i_{corr} **(mA·cm^{-2})**	β_c **(mV/dec)**	β_a **(mV/dec)**	***IE*** **%**
Blank	–789	13.51	–267	55	–
0.5	–780	1.76	–216	29	86.97
1	–772	1.37	–214	26	89.85
2	–766	1.34	–299	23	90.08
3	–750	1.21	–299	26	91.04

According to the results obtained (Figure 1 and Table 1), both anodic and cathodic current decrease with increasing concentration of the extract with a slight displacement of the corrosion potential to cathodic values. This behavior translates the capacity of extracts to inhibit aluminum corrosion in 1 M HCl solution. In acid medium, the cathodic process represents the reduction of hydrogen ions to produce hydrogen molecules or reduction of

oxygen, while the anodic corrosion process is the passage of metal ions from the solid metal to the solution (dissolution of aluminum). As seen previously, i_{corr} decreases in the presence of inhibitor, and this decrease results in an increase in the inhibition efficiency *IE*%. This may be due to the adsorption of the inhibitor molecules of the extract on the active sites of the aluminum surface and formation of an inhibitor film on the metal surface, therefore the corrosion reactions (anodic and cathodic) of aluminum are hindered. The inhibition efficiency of the extract (3 g/L) reached a maximum of 91.04%, indicating that this extract is a good inhibitor of aluminum in 1.0 M HCl. Addition of the extract to 1.0 M HCl solution did not result in a remarkable shift in the E_{corr} value from the blank. This observation clearly shows that this inhibitor can be classified as a mixed-type inhibitor at all its concentrations. However, since the cathodic current densities decrease much more than those of the anodic current, the extract acts as a mixed-type inhibitor with cathodic priority [51].

3.2.2. Electrochemical impedance spectroscopy

The purpose of using the electrochemical impedance diagrams at the corrosion potential and at different inhibitor concentrations is to complete and study the corrosion mechanism of the aluminum alloy in 1 M HCl medium.

Figure 3 shows the EIS Nyquist diagrams at different concentrations of the extract, and the associated electrochemical parameters are shown in Table 3.

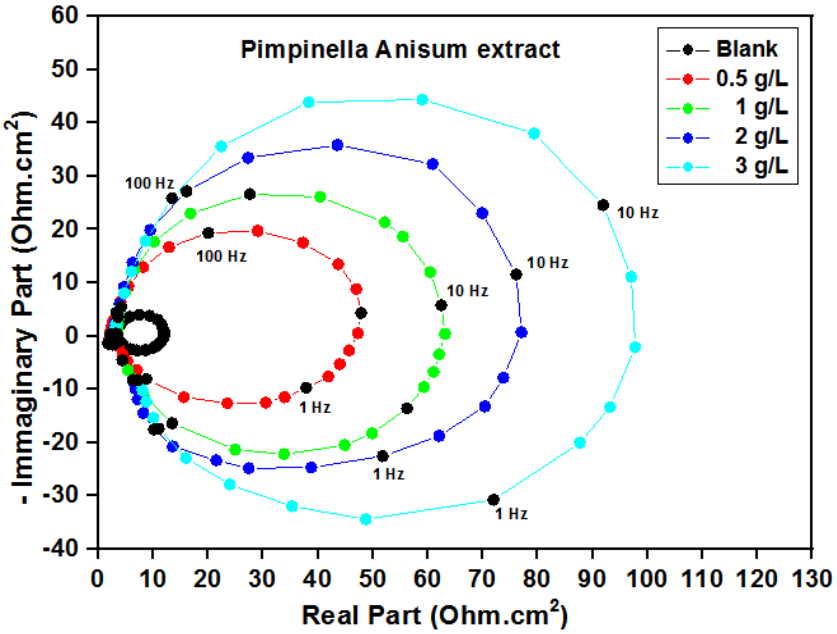

Figure 3. EIS Nyquist diagrams of aluminum in 1 M HCl without and with different concentrations of *Pimpinella Anisum* extract.

Table 3. Electrochemical parameters of aluminum corrosion in 1.0 M HCl solution at different inhibitor concentrations.

Concentration (g/L)	R_s (Ohm)	R_{ct} (Ohm)	CPE (μF)	L (H)	R_i (Ohm)	R_p (Ohm)	IE %
Blank	2.52	8.59	50.95	16.47	0.58	0.54	–
0.5	2.17	44.78	45.78	23.36	2.85	2.67	79.72
1	2.29	60.71	39.93	37.50	3.08	2.93	81.56
2	2.77	75.88	34.51	19.71	3.23	3.09	82.52
3	2.86	94.76	31.92	24.64	5.58	5.26	89.34

Analysis of Figure 3 shows that as the inhibitor concentration rises, the semi-circle diameter rises indicating that the charge transfer process is the primary factor controlling aluminum corrosion. In the presence of the inhibitor, the shape is maintained for all concentrations tested, indicating that there is no change in the corrosion mechanism, to be precise the whole diagram appears as an elliptical shape which agrees with a recent work on aluminum in HCl [52]. A similar form is also found for aluminum in the acid solution inhibited by oxime compounds [53].

According to numerous studies [54–56], in the absence of an inhibitor, the capacitive loop at high frequency (HF) could be attributed to the formation of an oxide layer on Al. It is reasonable to assume that the electrode surface is covered with an oxide layer during the *ex situ* pretreatment of the electrode, but it is difficult to produce the oxide on the surface of aluminum since it is re-passivated very quickly in the presence of oxygen. The capacitive loop at HF corresponds to the interfacial reactions, exactly, the oxidation of aluminum at the metal/oxide/electrolyte interface [57]. In the present system, the oxide layer formed is dissolved in the acid medium, therefore the formation of Al^+ ions at the metal/oxide interface and their migration through the oxide/solution interface where they oxidize to Al^{3+} is the principal dissolution process of aluminum. In the presence of the inhibitor, the [metal–oxide–hydroxide–inhibitor]$_{ads}$ complex could also be formed. The fact that all these processes are illustrated by only one loop can be attributed either to the supposition that one process dominates and therefore, excludes the other processes or to the overlapping of the loops of processes [58]. The origin of the inductive loop is unknown, different research was done to give an exact explanation for the source of this loop. Adsorbed charged intermediates could be a cause of this loop [59], also it can be related to adsorbed H^+ according to the research that was done by W. Lenderink *et al*. [60]. Other researchers considered that the inductive part can be determined by the relaxation process of Cl^- or dissolution of Al [54]. It may be similarly attributed to the redissolution of the oxide on the surface of aluminum at low frequencies [10].

The electrical circuit shown in Figure 4 was employed to simulate the results of EIS. It was composed by five elements: R_s, $R_{ct,}$ and R_i are the solution resistance, charge transfer

resistance, and inductive resistance respectively. *L* is the inductance that is associated with the inductive part. It is important to hint that the double layer capacitance C_{dl} value is affected by imperfections and inhomogeneous of the surface and to have a good simulation, the use of a constant phase element CPE is necessary [52].

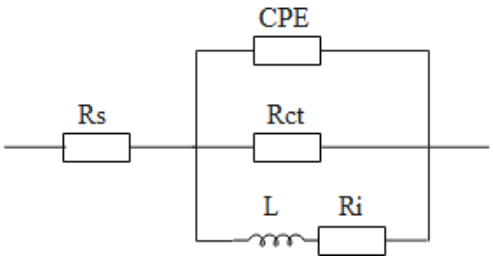

Figure 4. Equivalent circuit used to model the impedance diagrams.

3.3. Adsorption isotherm

To get more information on the interaction between the aluminum surface and the inhibitor, various adsorption isotherms were applied to fit the coverage θ values, but the best fit was found to obey the Langmuir adsorption isotherm which is represented in Figure 5.

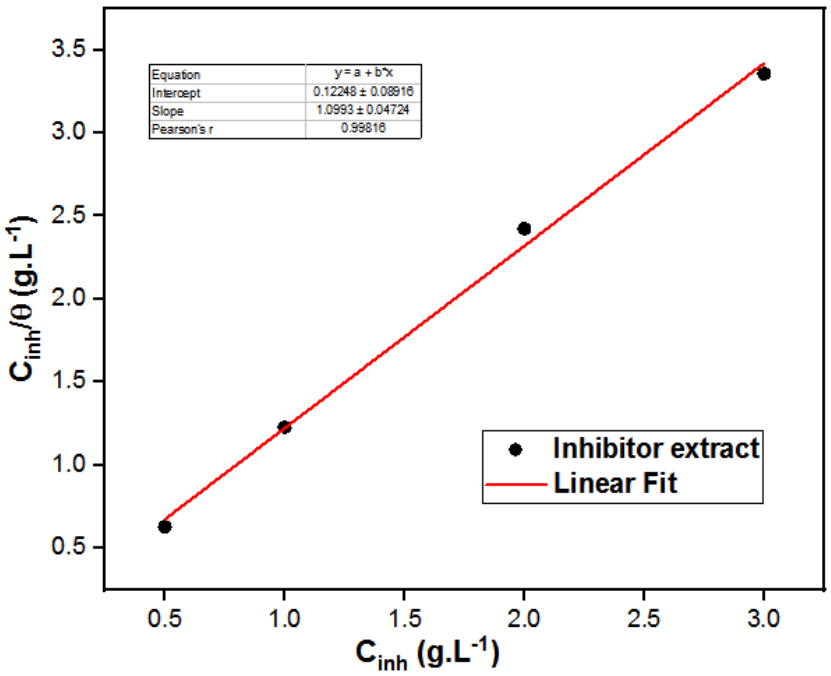

Figure 5. Langmuir adsorption isotherm of *Pimpinella Anisum* extract on aluminum surface in 1 M HCl acid solution.

3.4. Scanning electron microscopy

The characterization of the metal surface was carried out by SEM/EDX technique to reinforce the results; the obtained results are recorded in Figures 6 and 7 before and after

immersion in 1 M HCl solution for 24 hours in the absence and in the presence of 3 g/L of the inhibitor.

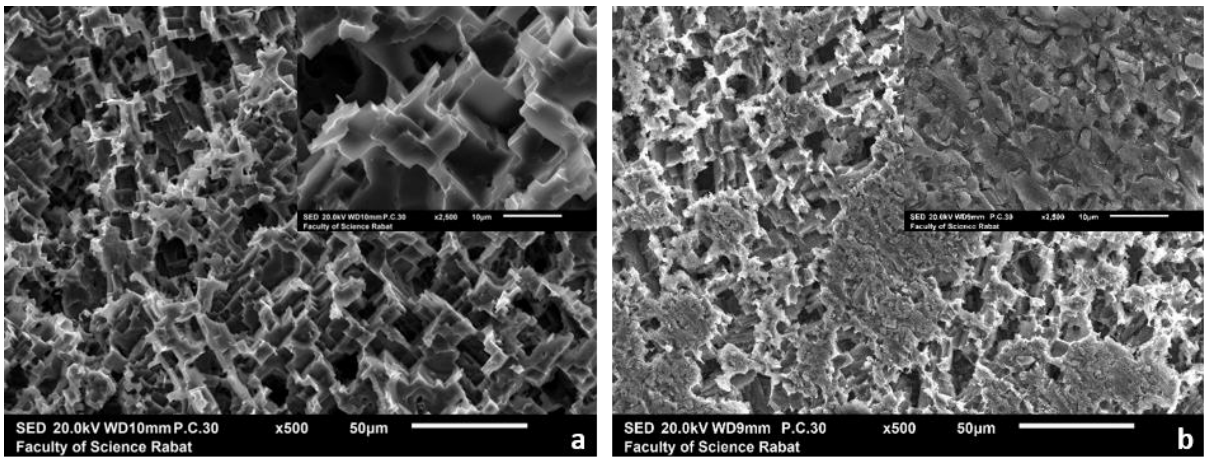

Figure 6. SEM images of aluminum surface after immersion in 1 M HCl (a) and inhibited by *Pimpinella Anisum* extract (b).

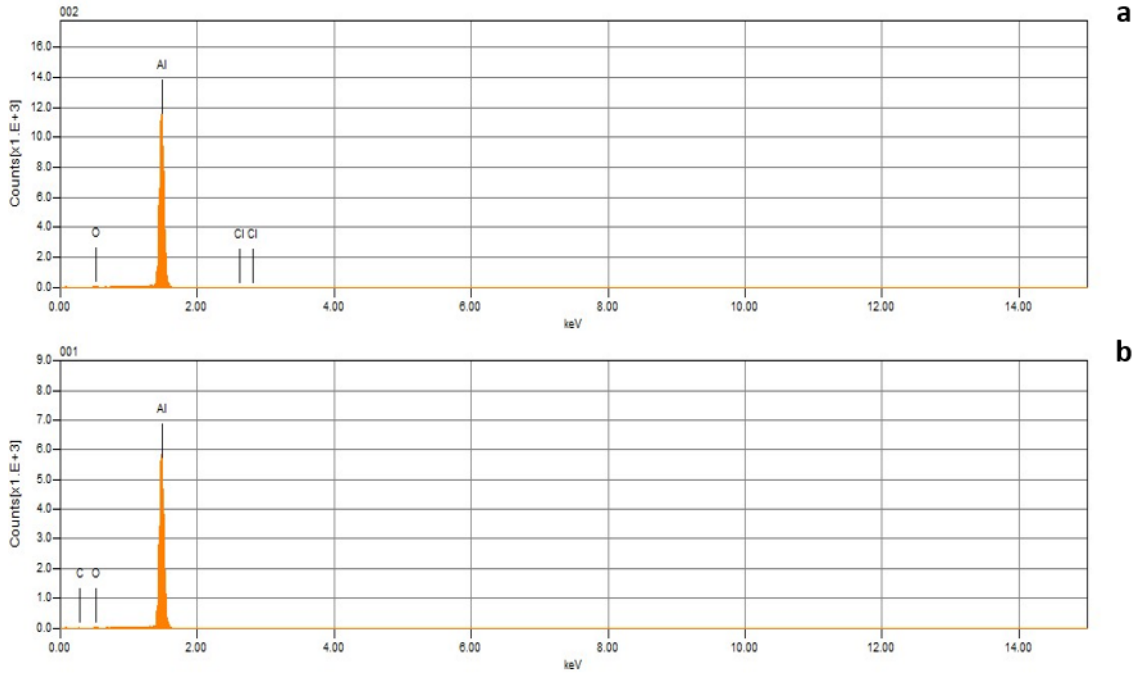

Figure 7. EDX elemental analysis spectra for aluminum alloy after immersion in 1 M HCl (8a) and inhibited by *Pimpinella Anisum* extract (8b).

After immersion in uninhibited 1 M HCl solution for 24 h, an aggressive attack of the corrosive medium appears on the surface of aluminum (Figure 6a). Moreover, the corrosion products resemble cubic morphology and are very uneven. The corroded layer is very porous and rough, and demonstrates some black holes. Through these black holes, the aggressive ions can penetrate deep into the fresh aluminum surface and then attack it to form corrosion

products. On other hand, the micrograph of an inhibited specimen shown in Figure 6b reveals that there is much less damage on the aluminum surface, which further confirms the inhibition ability of our extract.

The EDS of the aluminum alloy after immersion in 1 M HCl (Figure 7a) showed clear O and Al peaks, which indicates that the film formed on the alloy surface was mainly composed of aluminum oxides and hydroxides. The spectra in Figure 7b show a decrease in the aluminum signal intensity.

3.5. DFT results

The HOMO and LUMO (Figure 8) distribution and their symmetry have renowned as fundamental parameters for determining the activity of a molecule and guessing on the development of chemical reactions [47, 61]. The HOMO renders the parts of the molecule that have a liability to donate electrons to electrophilic species while the LUMO points to the molecule areas with a high predilection to receive electrons from nucleophilic species.

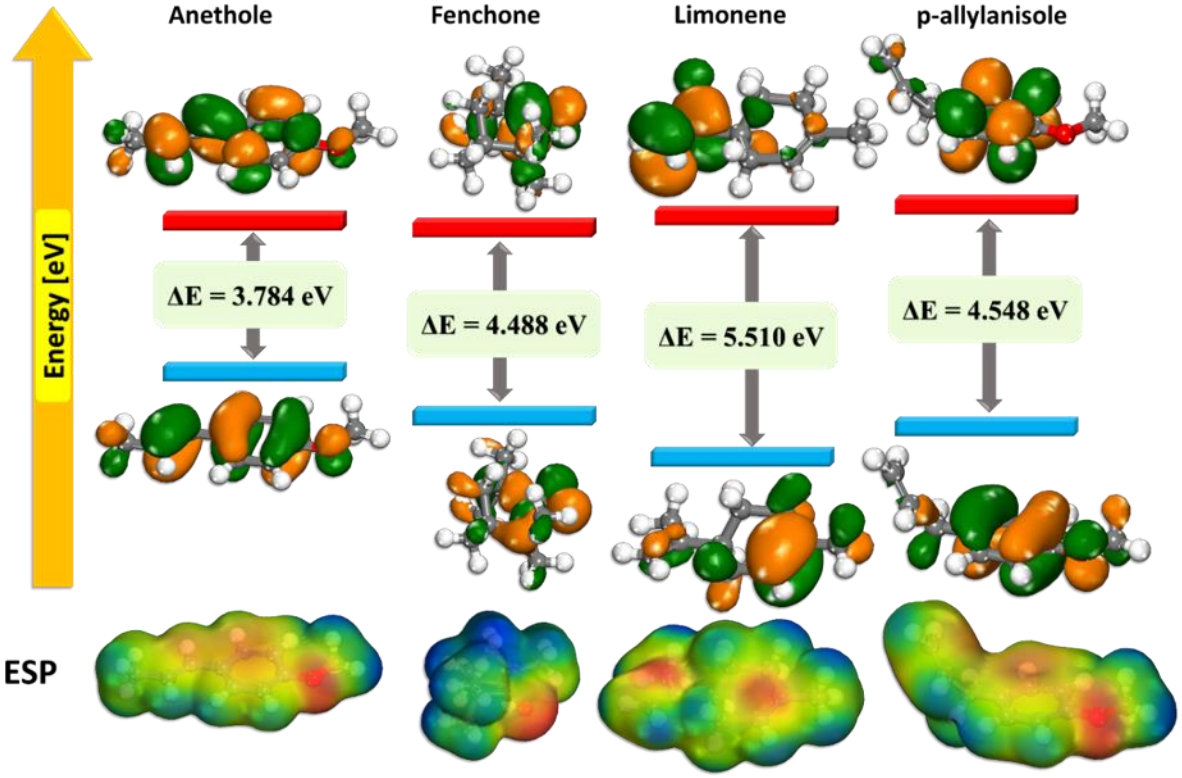

Figure 8. HOMO, LUMO surfaces, and ESP of the anethole, fenchone, limonene, and *p*-allylanisole inhibitors

The HOMO and LUMO OM and MEP of the anethole, fenchone, limonene, and *p*-allylanisole inhibitors are shown in Figure 8 and frequent DFT indices are given in Table 5.

The boundary MO's show that the HOMO is distributed mainly over the central ring and the nearby oxygen atoms in the anethole inhibitor; in the case of fenchone, the HOMO

density is concentrated mainly near the O atom; for limonene HOMO is uniformly distributed throughout the system and for *p*-allylanisole, most of the HOMO density is in the central part of the molecule. On the other hand, in the anethole the LUMO is distributed throughout the structure of the molecule; for fenchone, the LUMO is concentrated near the O atom; for limonene, it is focused on a part of the attached methyl groups, while for *p*-allylanisole the LUMO density is centered in the middle part of the molecule. The solid significant value of HOMO for the inhibitor molecules points toward their ability to interact with Al(111) surface by electron donation and acceptance [43, 62–65].

Table 5. Calculated theoretical chemical parameters for anethole, fenchone, limonene and *p*-allylanisole inhibitors.

Theoretical parameters	Anethole	Fenchone	Limonene	*p*-Allylanisole
HOMO	–4.9890	–5.6960	–5.5300	–5.3550
LUMO	–1.2050	–1.2080	0.0270	–0.8070
Δ*E* (HOMO–LUMO)	3.7840	4.4880	5.5570	4.5480
Ionization energy (*I*)	4.9890	5.6960	5.5300	5.3550
Electron affinity *A*)	1.2050	1.2080	–0.0270	0.8070
Electronegativity (χ)	3.0970	3.4520	2.7515	3.0810
Global hardness (η)	1.8920	2.2440	2.7785	2.2740
Chemical potential (π)	–3.0970	–3.4520	–2.7515	–3.0810
Global softness (σ)	0.5285	0.4456	0.3599	0.4398
Global electrophilicity (ω)	2.5347	2.6551	1.3624	2.0872
Electrodonating (ω–) power	4.3197	4.6616	3.0854	3.9119
Electroaccepting (ω+) power	1.2227	1.2096	0.3339	0.8309
Net electrophilicity (Δω+–)	0.9912	0.9951	0.0098	0.5753
Fraction of transferred electrons (Δ*N*)	0.3073	0.1800	0.2715	0.2592
Energy from Inhibitor to Metals	0.0204	–0.0200	0.0649	0.0193
Δ*E* back-donation	–0.4730	–0.5610	–0.6946	–0.5685

This activity is also evident from the relatively low electron affinity and high values of ionization potential, leading to a similar capability in electron exchange capacity. In agreement with this, the relatively high value of chemical softness and low value of hardness are also probable values supporting that the inhibitors are highly reactive entities that possess adsorptive tendency when adjacent to metal surfaces [66–69].

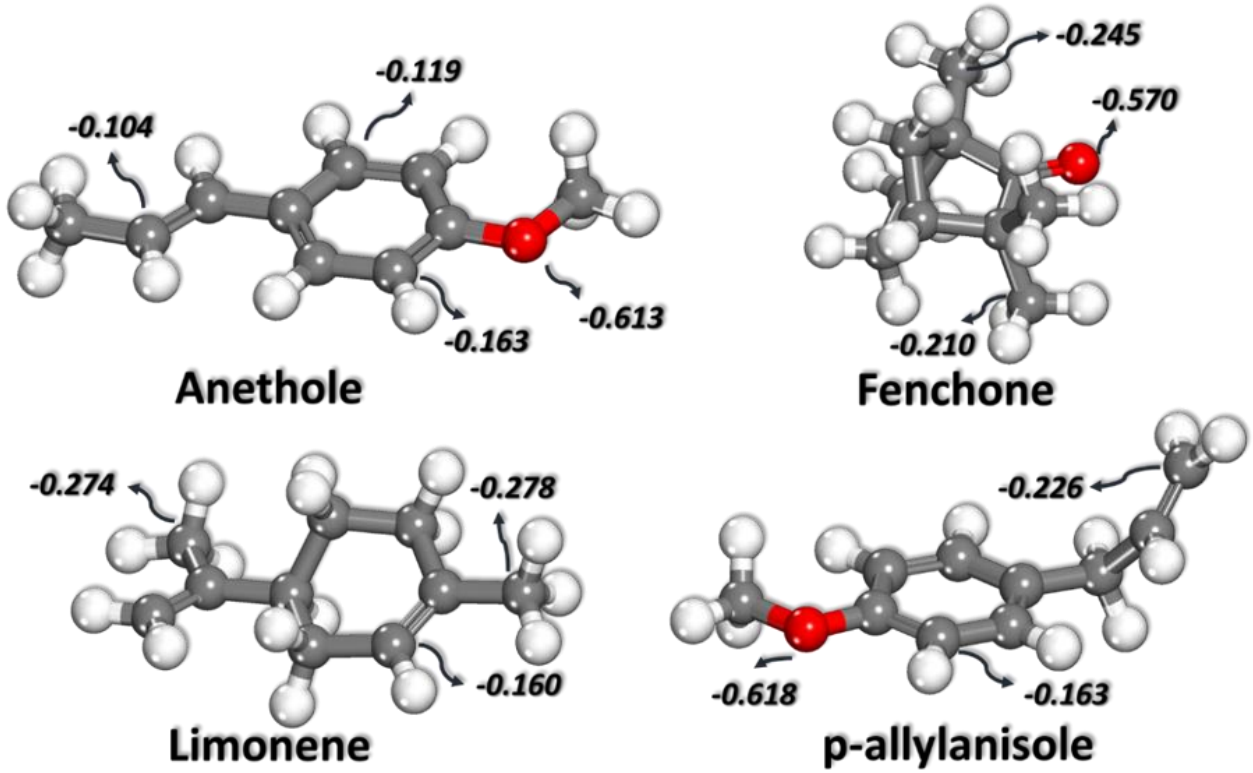

Figure 9. Optimized structures of the anethole, fenchone, limonene and *p*-allylanisole inhibitors and their Mulliken atomic charges (MAC).

MAC are trustworthy, according to the sites (atoms) of inhibitors responsible for adsorption to metals. The interaction between the Al(111) surface and the inhibitor molecules is routinely considered to be fruitful at the atom with the highest negative charge [68]. The MAC for all the studied inhibitors is shown in Figure 9. The maximum negative charges are located at the O atoms of the inhibitors, which means that these centers have the highest electron density and interact with the metal surface. This is also evident in Figure 9, where the molecular electrostatic potential (MEP) for the inhibitors is shown (area in red).

3.6. Monte Carlo and Molecular dynamic simulations

Figure 10 shows the lowest energy configurations for the inhibitors anethole, fenchone, limonene and *p*-allylanisole at the metal surface in the simulated corrosive media (as chosen above). The adsorption geometries of the inhibitors (supported by Mulliken charges) indicate that this process is assisted by nitrogen and oxygen atoms. This adsorption behavior is responsible for the formation of an anticorrosive layer on the metal surface that protects the material.

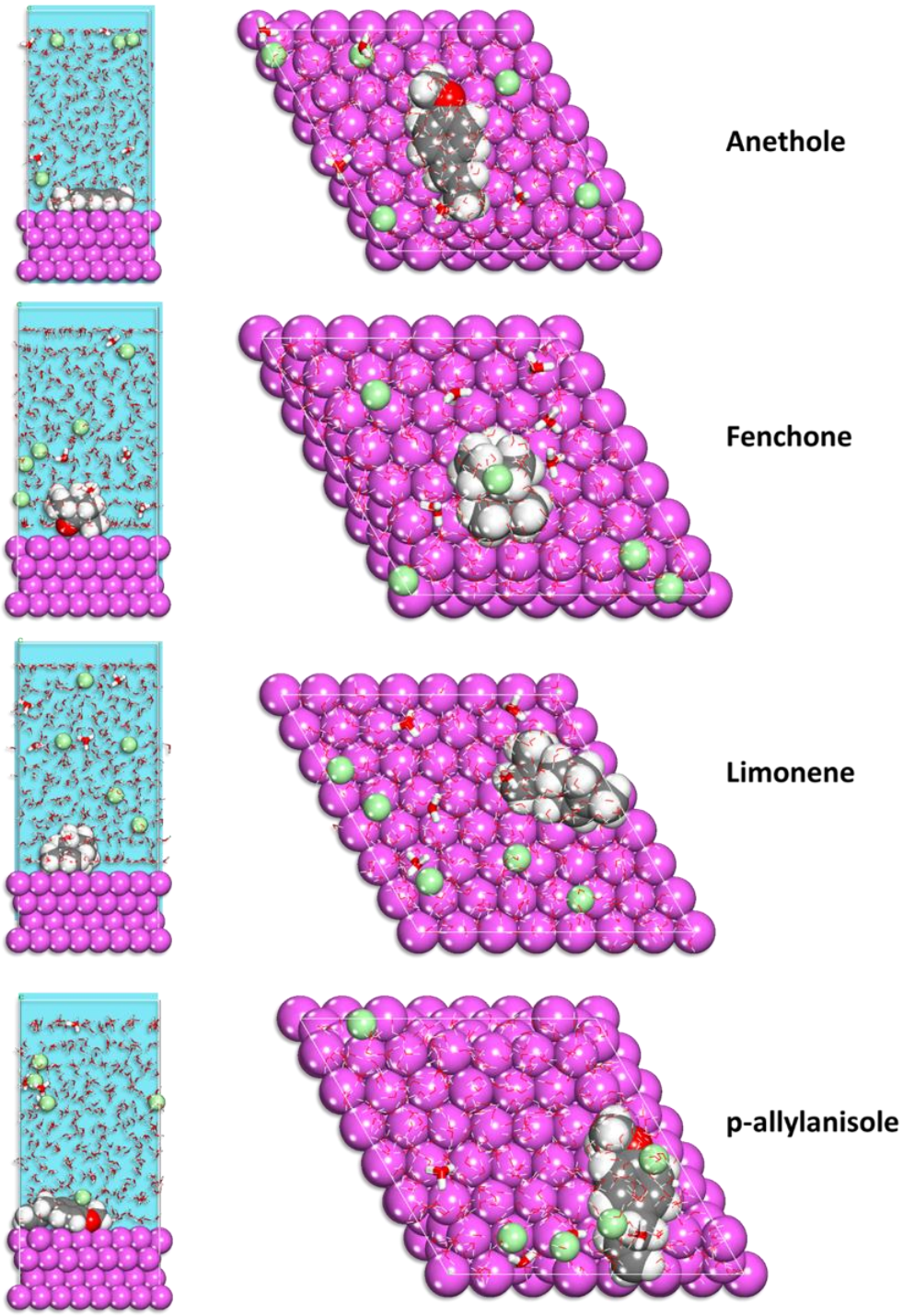

Figure 10. Final MC poses of the lowest adsorption configurations for anethole, fenchone, limonene and *p*-allylanisole inhibitors onto the Al(111) surface.

The assessment of the interaction of the inhibitor molecules anethole, fenchone, limonene and *p*-allylanisole with the metal surface is done by calculating the adsorption energies using the following equation (5):

$$E_{ads} = E_{total} - [E_{(surface + water)} + E_{(anethole,fenchone,limonene\ or\ p\text{-}allylanisole)}] + E_{water} \quad (5)$$

where: E_{total} is the total energy of the system as a result of inhibitor-metal interaction; $E_{surface + water}$ and $E_{anethole, fenchone, limonene or p-allylanisole + water}$ is system energy in the absence and presence of anethole, fenchone, limonene and *p*-allylanisole inhibitors.

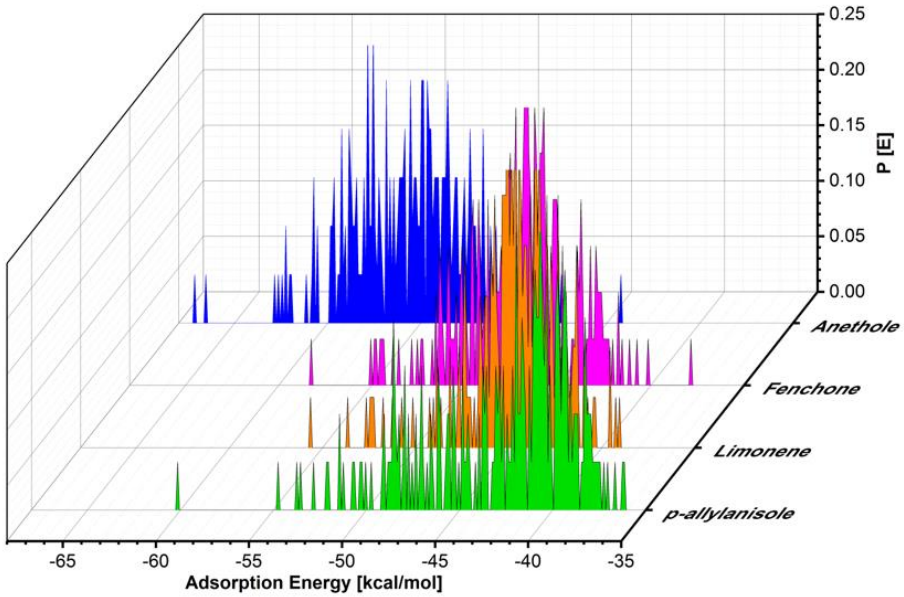

Figure 11. Distribution of the adsorption energies for anethole, fenchone, limonene and *p*-allylanisole inhibitors onto the Al(111) surface obtained using MC.

The Monte Carlo calculations (Figure 11) are in good line with the experimental results. The negative value of the adsorption energy supports the spontaneity of the adsorption process [68]. All of the inhibitors interact strongly with the Al(111) surface: Anethole (E_{ads} = –61.92 kcal/mol) > Fenchone (E_{ads} = –54.56 kcal/mol) > Limonene (E_{ads} = –52.21 kcal/mol) > *p*-allylanisole (E_{ads} = –50.30 kcal/mol) (energy terms during MC search and the 10 most stable energies values obtained from MC are presented in Supporting Information).

MD simulations possess the ability to trail and seizure the dynamics of the adsorption of the studied inhibitors on the metal surface. Figure 12 illustrates the latest configurations of inhibitors on the metal surface.

From Figure 12 (MD) and Figure 11 (MC), the inhibitors are strongly adsorbed on the surface. From the drawings of adsorbed inhibitors, it is evident that the inhibitors are adsorbed flatly on the surface by orienting their oxygen atoms towards the surface (as directed by Mulliken charges). This conclusion is also supported by the analysis of the Radial Distribution Function (RDF), which calculates the oxygen atoms from the horizontal of the metal surface and is shown in Figure 13.

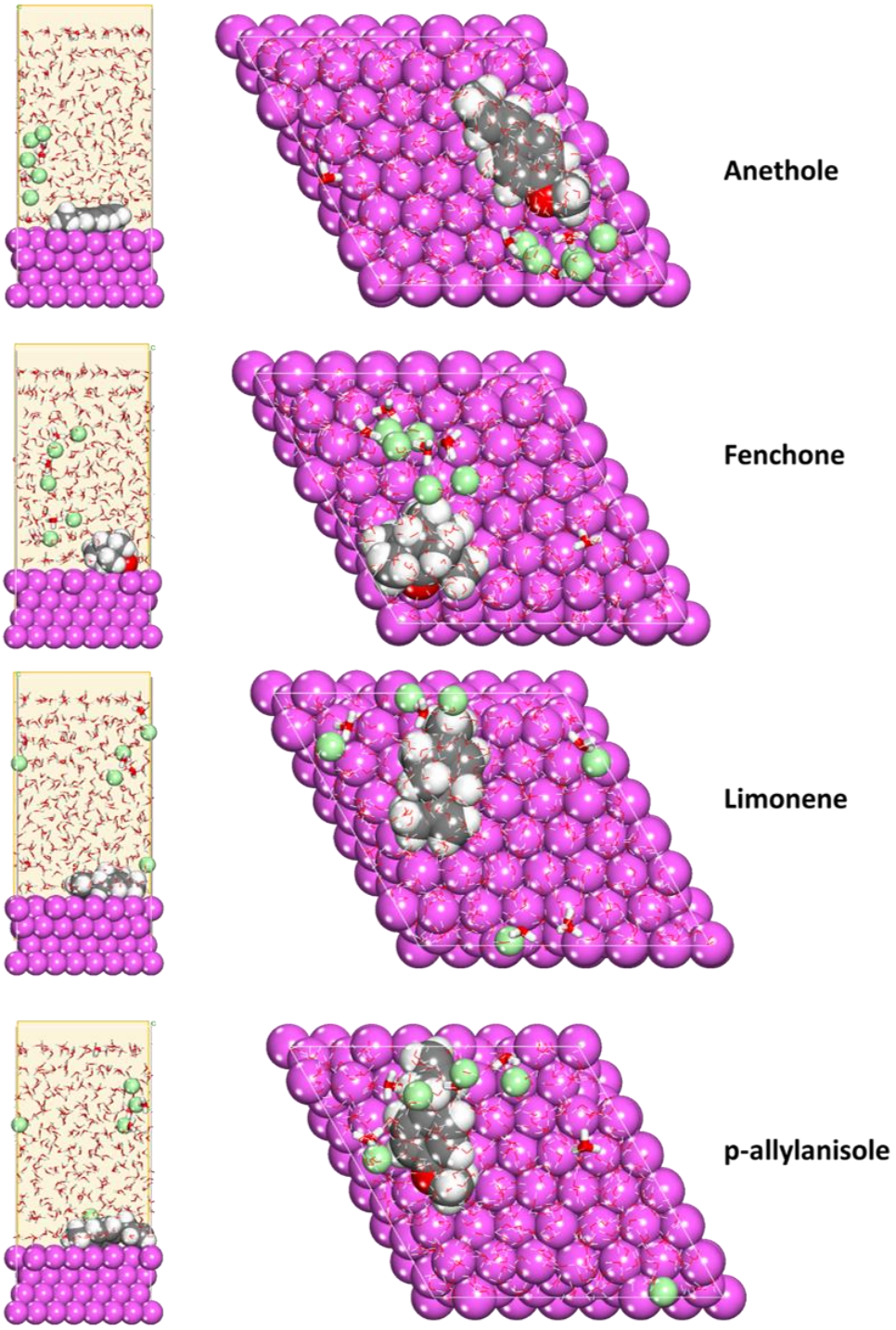

Figure 12. Final MD poses of the lowest adsorption configurations for anethole, fenchone, limonene and *p*-allylanisole inhibitors onto the Al(111) surface.

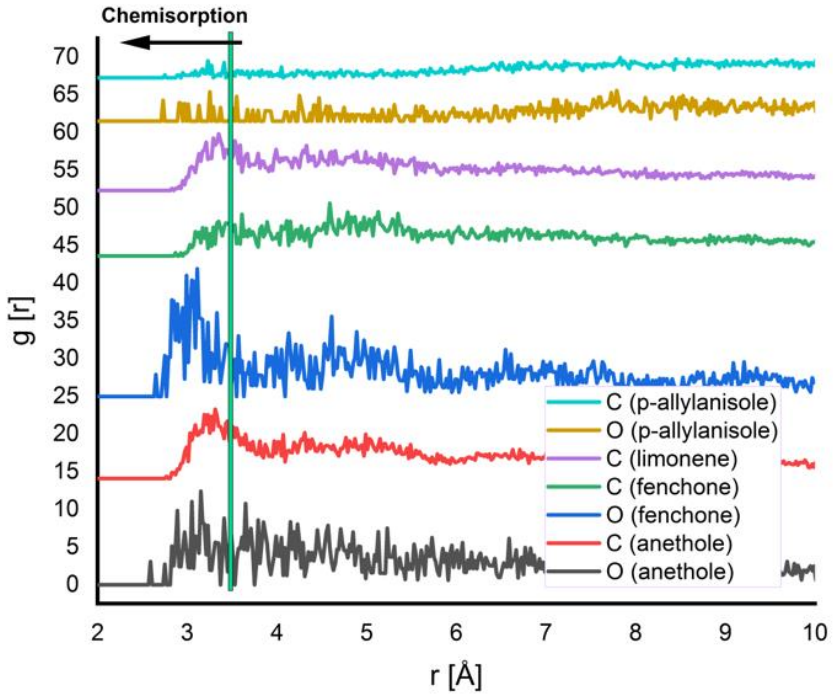

Figure 13. RDF oxygen atoms of anethole, fenchone, limonene and *p*-allylanisole inhibitors onto the Al(111) surface obtained by means of MD.

It is agreed that if the peak appears in the RDF curve of certain atom(s) and the surface in the range of 1 and 3.5 Å, it is a strong suggestion that chemisorption is taking place, while in the case of physisorption RDF peaks, the presence at larger distances (typically larger than 3.5 Å) is to be expected [45, 62]. The RDF of the oxygen and carbon atoms (Figure 6) for anethole, fenchone, limonene and *p*-allylanisole inhibitors is under 3.0 Å describing a chemisorption of the inhibitor on the metal surface. The results obtained from MD and the corresponding RDF analysis confirm once again (as the obtained experimental results and MC calculations show) the robust predisposition of the inhibitors to adsorb and protect the metal due to their extraordinary attraction to bring and take electrons to the metal surface [64, 66].

4. Conclusion

The results obtained show that the aqueous extract of *Pimpinella Anisum* is an effective and potential inhibitor of aluminum in 1 M HCl. The inhibition efficiency increases with the increase in the extract concentration to reach 92% for a concentration of 3 g/L of the inhibitor. The polarization curves illustrate that the extract acts as a mixed inhibitor. The inhibition is normally caused by adsorption of molecules from the aqueous extract to the aluminum surface. These results are confirmed by the electrochemical impedance plots. SEM/EDX results show that the aluminum surface is covered with an inhibitor film; this film is responsible for hindering the reduction of H^+ ions and for inhibiting the dissolution

of aluminum in 1 M HCl. The DFT calculations were able to determine the adsorption centers of the inhibitors. Moreover, the MC and MD calculations indicate the strong adsorption interaction of anethole, fenchone, limonene and *p*-allylanisole inhibitors towards the metal surface and provide molecular facts about the adsorption behavior (geometry) and adsorption energy of these inhibitors on aluminum surface. The theoretical results offered (DFT, MC and MD) are in general agreement with the experimental results.

Reference

1. H. Ashassi-Sorkhabi, Z. Ghasemi and D. Seifzadeh, The inhibition effect of some amino acids towards the corrosion of aluminum in 1 M HCl+1 M H_2SO_4 solution, *Appl. Surf. Sci*., 2005, **249**, no. 1–4, 408–418. doi: 10.1016/j.apsusc.2004.12.016
2. Y.-T. Du, H.-L. Wang, Y.-R. Chen, H.-P. Qi and W.-F. Jiang, Synthesis of baicalin derivatives as eco-friendly green corrosion inhibitors for aluminum in hydrochloric acid solution, *J. Environ. Chem. Eng*., 2017, **5**, no. 6, 5891–5901. doi: 10.1016/j.jece.2017.11.004
3. P.C. Okafor, E.E. Ebenso and U.J. Ekpe, Inhibition of the acid corrosion of aluminium by some derivatives of thiosemicarbazone, *Bull. Chem. Soc. Ethiop*., 2004, **18**, no. 2, 181–192. doi: 10.4314/bcse.v18i2.61442
4. E.A. Noor, Potential of aqueous extract of *Hibiscus sabdariffa* leaves for inhibiting the corrosion of aluminum in alkaline solutions, *J. Appl. Electrochem*., 2009, **39**, no. 9, 1465–1475. doi: 10.1007/s10800-009-9826-1
5. P.S. Desai, *Calotropis gigantea* Leaves Ark Used as Corrosion Inhibitor for Aluminum in Hydrochloric Acid, *Pharm. Chem*., 2018, **10**, no. 1, 7–12.
6. K. Xhanari and M. Finšgar, Organic corrosion inhibitors for aluminum and its alloys in chloride and alkaline solutions: A review, *Arab. J. Chem*., 2016, **12**, no. 8, 4646–4663. doi: 10.1016/j.arabjc.2016.08.009
7. D. Bouknana, B. Hammouti, S. Jodeh, M. Sbaa and H. Lgaz, Extracts of Olive Inflorescence Flower Pre-Anthesis, at Anthesis and Grain Pollen as Eco-Friendly Corrosion Inhibitor for Steel in 1M HCl Medium, *Anal. Bioanal. Electrochem*., 2018, **10**, no. 6, 751–777.
8. M.C. Anbarasi and K.S. Suruthi, Chrysanthemum Flower Extract as a Green Inhibitor for Aluminium Corrosion in Alkaline Medium, *Int. J. ChemTech Res*., 2018, **11**, no. 07, 37–44. doi: 10.20902/IJCTR.2018.110705
9. N. Chaubey, M.A. Quraishi and E.E. Ebenso, Corrosion inhibition of aluminium alloy in alkaline media by Neolamarkia Cadamba Bark extract as a green inhibitor, *Int. J. Electrochem. Sci*., 2015, **10**, no. 1, 504–518.
10. A. Ennouri, A. Lamiri and M. Essahli, Corrosion Inhibition of Aluminium in Acidic Media by Different Extracts of *Trigonellafoenum-graecum L* Seeds, *Port. Electrochim. Acta*, 2017, **35**, no. 5, 279–295. doi: 10.4152/pea.201705279
11. B.E.A. Rani and B.B.J. Basu, Green Inhibitors for Corrosion Protection of Metals and Alloys: An Overview, *Int. J. Corros*., 2012, 1–15. doi: 10.1155/2012/380217

12. A.Y. El-Etre, Inhibition of aluminum corrosion using Opuntia extract, *Corros. Sci*., 2003, **45**, no. 11, 2485–2495. doi: 10.1016/S0010-938X(03)00066-0
13. Y.P. Yee, S.N. Saud and E. Hamzah, Pomelo Peel Extract as Corrosion Inhibitor for Steel in Simulated Seawater and Acidic Mediums, *J. Mater. Eng. Perform*., 2020, **29**, no. 4, 2202–2215. doi: 10.1007/s11665-020-04774-1
14. M. Yeganeh, I. Khosravi-Bigdeli, M. Eskandari and S.R. Alavi Zaree, Corrosion Inhibition of l-Methionine Amino Acid as a Green Corrosion Inhibitor for Stainless Steel in the H_2SO_4 Solution, *J. Mater. Eng. Perform*., 2020, **29**, no. 6, 3983–3994. doi: 10.1007/s11665-020-04890-y
15. P. Muthukrishnan, B. Jeyaprabha and P. Prakash, Corrosion Inhibition and Adsorption Behavior of *Setaria verticillata* Leaf Extract in 1 M Sulphuric Acid, *J. Mater. Eng. Perform*., 2013, **22**, no. 12, 3792–3800. doi: 10.1007/s11665-013-0700-2
16. W. Sun, M.H. Shahrajabian and Q. Cheng, Anise (*Pimpinella anisum* L.), a dominant spice and traditional medicinal herb for both food and medicinal purposes, *Cogent Biol*., 2019, **5**, no. 1, 1673688. doi: 10.1080/23312025.2019.1673688
17. A.A. El Hosary, R.M. Saleh and A.M. Shams El Din, Corrosion inhibition by naturally occurring substances – I. The effect of *Hibiscus subdariffa* (karkade) extract on the dissolution of Al and Zn, *Corros. Sci*., 1972, **12**, no. 12, 897–904. doi: 10.1016/S0010-938X(72)80098-2
18. M.H. Boskabady and M. Ramazani-Assari, Relaxant effect of *Pimpinella anisum* on isolated guinea pig tracheal chains and its possible mechanism(s), *J. Ethnopharmacol*., 2001, **74**, no. 1, 83–88. doi: 10.1016/S0378-8741(00)00314-7
19. A. Shokri, T. Hatami and M. Khamforoush, Near critical carbon dioxide extraction of Anise (*Pimpinella Anisum* L.) seed: Mathematical and artificial neural network modeling, *J. Supercrit. Fluids*, 2011, **58**, no. 1, 49–57. doi: 10.1016/j.supflu.2011.04.011
20. H.S.A.A. Mohamed, W.S. Abdelgadir and A.Z.I. Almagboul, *In vitro* antimicrobial activity of Anise seed (*Pimpinella anisum* L.), *Int. J. Adv. Res*., 2015, **3**, no. 1, 359–367.
21. A. Al Maofari, S. El Hajjaji, A. Debbab, S. Zaydoun, B. Ouaki, R. Charof, Z. Mennane, A. Hakiki and M. Mosaddak, Chemical composition and antibacterial properties of essential oils of *pimpinella anisum* l. growing in Morocco and Yemen, *Sci. Study Res.: Chem. Chem. Eng., Biotechnol., Food Ind*., 2013, **14**, no. 1, 11–16.
22. R. Hänsel, O. Sticher and E. Steinegger, *Pharmakognosie – Phytopharmazie*, 6th ed., 1999, Berlin Heidelberg: Springer-Verlag.
23. E.L. Ponte, P.L. Sousa, M.V.A.P. Rocha, P.M.G. Soares, A.N. Coelho-de-Souza, J.H. Leal-Cardoso and A.M.S. Assreuy, Comparative study of the anti-edematogenic effects of anethole and estragole, *Pharmacol. Rep*., 2012, **64**, no. 4, 984–990. doi: 10.1016/S1734-1140(12)70895-2
24. K.M. Zohdy, M.M. Younes and H.A. Abdel-Rahman, Electrochemical Inhibition Studies on Carbon Steel in Acidic Medium *via* Friendly Anise Oil with Gamma-Irradiated Rays, *J. Transition Met. Complexes*, 2020, **3**, 1–6. doi: 10.32371/jtmc/246096

25. F. Bouhlal, N. Labjar, F. Abdoun, A. Mazkour, M. Serghini-Idrissi, M.E. Mahi, E.M. Lotfi, A. Skalli and S. El Hajjaji, Chemical and electrochemical studies of the inhibition performance of hydro-alcoholic extract of used coffee grounds (HECG) for the corrosion of C38 steel in 1 M hydrochloric acid, *Egypt. J. Pet*., 2020, **29**, no. 1, 45–52. doi: 10.1016/j.ejpe.2019.10.003
26. Z. Akounach, A. Al Maofari, A. El Yadini, S. Douche, M. Benmessaoud, B. Ouaki, M. Damej and S. El Hajjaji, Inhibition of Mild Steel Corrosion in 1.0 M HCl by Water, Hexane and Ethanol Extracts of *Pimpinella Anisum* Plant, *Anal. Bioanal. Electrochem*., 2018, **10**, no. 11, 1506–1524.
27. A.M. Nagiub, Electrochemical Noise Analysis for Different Green Corrosion Inhibitors for Copper Exposed to Chloride Media, *Port. Electrochim. Acta*, 2017, **35**, 201–210. doi: 10.4152/pea.201704201
28. H. Hosseinzadeh, M. Tafaghodi, S. Abedzadeh and E. Taghiabadi, Effect of Aqueous and Ethanolic Extracts of *Pimpinella anisum* L. Seeds on Milk Production in Rats, *J. Acupunct. Meridian Stud*., 2014, **7**, no. 4, 211–216. doi: 10.1016/j.jams.2013.10.004
29. A. Shojaii and M. Abdollahi Fard, Review of Pharmacological Properties and Chemical Constituents of *Pimpinella anisum*, *ISRN Pharm*., 2012, 510795. doi: 10.5402/2012/510795
30. M. Damej, D. Chebabe, M. Benmessaoud, A. Dermaj, H. Erramli, N. Hajjaji and A. Srhiri, Corrosion inhibition of brass in 3% NaCl solution by 3-methyl-1,2,4-triazol-5-thione, *Corros. Eng., Sci. Technol*., 2015, **50**, 103–107. doi: 10.1179/1743278214Y.0000000207
31. M. Damej, H. Benassaoui, D. Chebabe, M. Benmessaoud, H. Erramli, A. Dermaj, N. Hajjaji and A. Srhiri, Inhibition effect of 1,2,4-triazole-5-thione derivative on the Corrosion of Brass in 3% NaCl solution, *J. Mater. Environ. Sci*., 2016, **7**, no. 3, 738–745.
32. H. Lgaz, S. Masroor, M. Chafiq, M. Damej, A. Brahmia, R. Salghi, M. Benmessaoud, I.H. Ali, M.M. Alghamdi, A. Chaouiki and I.M. Chung, Evaluation of 2-mercaptobenzimidazole derivatives as corrosion inhibitors for mild steel in hydrochloric acid, *Metals*, 2020, **10**, 1–14. doi: 10.3390/met10030357
33. B. Delley, From molecules to solids with the DMol3 approach, *J. Chem. Phys*., 2000, **113**, 7756–7764. doi: 10.1063/1.1316015
34. J. Andzelm, R.D. King-Smith and G. Fitzgerald, Geometry optimization of solids using delocalized internal coordinates, *Chem. Phys. Lett*., 2001, **335**, 321–326. doi: 10.1016/S0009-2614(01)00030-6
35. J.P. Perdew, K. Burke and M. Ernzerhof, Generalized gradient approximation made simple, *Phys. Rev. Lett*., 1996, **77**, 3865–3868. doi: 10.1103/PhysRevLett.77.3865
36. A. Berisha, Interactions between the aryldiazonium cations and graphene oxide: A DFT study, *J. Chem*., 2019, 5126071. doi: 10.1155/2019/5126071

37. Y. Zhao and D.G. Truhlar, The M06 suite of density functionals for main group thermochemistry, thermochemical kinetics, noncovalent interactions, excited states, and transition elements: Two new functionals and systematic testing of four M06-class functionals and 12 other functionals, *Theor. Chem. Acc*., 2008, **120**, 215–241. doi: 10.1007/s00214-007-0310-x
38. R. Peverati and D.G. Truhlar, Performance of the M11 and M11-L density functionals for calculations of electronic excitation energies by adiabatic time-dependent density functional theory, *Phys. Chem. Chem. Phys*., 2012, **14**, 11363–11370. doi: 10.1039/c2cp41295k
39. M. Ben Hadj Ayed, T. Osmani, N. Issaoui, A. Berisha, B. Oujia and H. Ghalla, Structures and relative stabilities of $Na^{+}Ne_n$ (n = 1–16) clusters *via* pairwise and DFT calculations, *Theor. Chem. Acc*., 2019, **138**, 84. doi: 10.1007/s00214-019-2476-4
40. Y. Inada and H. Orita, Efficiency of numerical basis sets for predicting the binding energies of hydrogen bonded complexes: Evidence of small basis set superposition error compared to Gaussian basis sets, *J. Comput. Chem*., 2008, **29**, 225–232. doi: 10.1002/jcc.20782
41. A. Berisha, First principles details into the grafting of aryl radicals onto the free-standing and borophene/Ag(111) surfaces, *Chem. Phys*., 2021, **544**, 111124. doi: 10.1016/j.chemphys.2021.111124
42. A. Molhi, R. Hsissou, M. Damej, A. Berisha, V. Thaçi, A. Belafhaili, M. Benmessaoud, N. Labjar and S. El Hajjaji, Contribution to the corrosion inhibition of C38 steel in 1 M hydrochloric acid medium by a new epoxy resin PGEPPP, *Int. J. Corros. Scale Inhib*., 2021, **10**, no. 1, 399–418. doi: 10.17675/2305-6894-2021-10-1-23
43. M. El Faydy, F. Benhiba, A. Berisha, Y. Kerroum, C. Jama, B. Lakhrissi, A. Guenbour, I. Warad and A. Zarrouk, An experimental-coupled empirical investigation on the corrosion inhibitory action of 7-alkyl-8-Hydroxyquinolines on C35E steel in HCl electrolyte, *J. Mol. Liq*., 2020, **317**, 113973. doi: 10.1016/j.molliq.2020.113973
44. M. Damej, S. Kaya, B. El Ibrahimi, H.S. Lee, A. Molhi, G. Serdaroğlu, M. Benmessaoud, I.H. Ali, S. El Hajjaji and H. Lgaz, The corrosion inhibition and adsorption behavior of mercaptobenzimidazole and bis-mercaptobenzimidazole on carbon steel in 1.0 M HCl: Experimental and computational insights, *Surf. Interfaces*, 2021, **24**, 101095. doi: 10.1016/j.surfin.2021.101095
45. A. Mazkour, S. El Hajjaji, N. Labjar, E.M. Lotfi and M. El Mahi, Corrosion Inhibition Effect of 5-Azidomethyl-8- Hydroxyquinoline on AISI 321 Stainless Steel in Phosphoric Acid Solution, *Int. J. Electrochem. Sci*., 2021, **16**, 210336. doi: 10.20964/2021.03.03
46. H. Sun, Z. Jin, C. Yang, R.L.C. Akkermans, S.H. Robertson, N.A. Spenley, S. Miller and S.M. Todd, COMPASS II: extended coverage for polymer and drug-like molecule databases, *J. Mol. Model*., 2016, **22**, 1–10. doi: 10.1007/s00894-016-2909-0
47. A. Berisha, Experimental, Monte Carlo and Molecular Dynamic Study on Corrosion Inhibition of Mild Steel by Pyridine Derivatives in Aqueous Perchloric Acid, *Electrochem*, 2020, **1**, 188–199. doi: 10.3390/electrochem1020013

48. S. Abbout, M. Zouarhi, D. Chebabe, M. Damej, A. Berisha and N. Hajjaji, Galactomannan as a new bio-sourced corrosion inhibitor for iron in acidic media, *Heliyon*, 2020, **6**, e03574. doi: 10.1016/j.heliyon.2020.e03574
49. M. Damej, M. Benmessaoud, S. Zehra, S. Kaya, H. Lgaz, A. Molhi, N. Labjar, S. El Hajjaji, A.A. Alrashdi and H.S. Lee, Experimental and theoretical explorations of S-alkylated mercaptobenzimidazole derivatives for use as corrosion inhibitors for carbon steel in HCl, *J. Mol. Liq*., 2021, **331**, 115708. doi: 10.1016/j.molliq.2021.115708
50. M. Rbaa, M. Ouakki, M. Galai, A. Berisha, B. Lakhrissi, C. Jama, I. Warad and A. Zarrouk, Simple preparation and characterization of novel 8-Hydroxyquinoline derivatives as effective acid corrosion inhibitor for mild steel: Experimental and theoretical studies, *Colloids Surf., A*, 2020, **602**, 125094. doi: 10.1016/j.colsurfa.2020.125094
51. N. Nnaji, N. Nwaji, J. Mack and T. Nyokong, Corrosion Resistance of Aluminum against Acid Activation: Impact of Benzothiazole-Substituted Gallium Phthalocyanine, *Molecules*, 2019, **24**, no. 1, 207. doi: 10.3390/molecules24010207
52. X. Li, S. Deng and H. Fu, Inhibition by tetradecylpyridinium bromide of the corrosion of aluminium in hydrochloric acid solution, *Corros. Sci*., 2011, **53**, no. 4, 1529–1536. doi: 10.1016/j.corsci.2011.01.032
53. X. Li, S. Deng and X. Xie, Experimental and theoretical study on corrosion inhibition of oxime compounds for aluminium in HCl solution, *Corros. Sci*., 2014, **81**, 162–175. doi: 10.1016/j.corsci.2013.12.021
54. E.A. Noor, Evaluation of inhibitive action of some quaternary N-heterocyclic compounds on the corrosion of Al–Cu alloy in hydrochloric acid, *Mater. Chem. Phys*., 2009, **114**, no. 2–3, 533–541. doi: 10.1016/j.matchemphys.2008.09.065
55. S.S. Abd El Rehim, H.H. Hassan and M.A. Amin, Corrosion inhibition study of pure Al and some of its alloys in 1.0 M HCl solution by impedance technique, *Corros. Sci*., 2004, **46**, no. 1, 5–25. doi: 10.1016/S0010-938X(03)00133-1
56. I.B. Obot and N.O. Obi-Egbedi, Inhibition of Aluminium Corrosion in Hydrochloric Acid Using Nizoral and the Effect of Iodide Ion Addition, *J. Chem.*, 2010, **7**, no. 3, 837–843. doi: 10.1155/2010/345168
57. C.M.A. Brett, On the electrochemical behaviour of aluminium in acidic chloride solution, *Corros. Sci*., 1992, **33**, no. 2. 203–210. doi: 10.1016/0010-938X(92)90145-S
58. S. Deng and X. Li, Inhibition by *Jasminum nudiflorum* Lindl. leaves extract of the corrosion of aluminium in HCl solution, *Corros. Sci*., 2012, **64**, 253–262. doi: 10.1016/j.corsci.2012.07.017
59. M.A. Amin, Q. Mohsen and O.A. Hazzazi, Synergistic effect of I^- ions on the corrosion inhibition of Al in 1.0 M phosphoric acid solutions by purine, *Mater. Chem. Phys*., 2009, **114**, no. 2–3, 908–914. doi: 10.1016/j.matchemphys.2008.10.057
60. H.J.W. Lenderink, M.V.D. Linden and J.H.W. De Wit, Corrosion of aluminium in acidic and neutral solutions, *Electrochim. Acta*, 1993, **38**, no. 14, 1989–1992. doi: 10.1016/0013-4686(93)80329-X

61. A. Berisha, F.F.I.F.I. Podvorica, V. Mehmeti, F. Syla and D. Vataj, Theoretical and experimental studies of the corrosion behavior of some thiazole derivatives toward mild steel in sulfuric acid media, *Maced. J. Chem. Chem. Eng*., 2015, **34**, 287–294. doi: 10.20450/mjcce.2015.576
62. R. Hsissou, S. Abbout, A. Berisha, M. Berradi, M. Assouag, N. Hajjaji and A. Elharfi, Experimental, DFT and molecular dynamics simulation on the inhibition performance of the DGDCBA epoxy polymer against the corrosion of the E24 carbon steel in 1.0 M HCl solution, *J. Mol. Struct*., 2019, **1182**, 340–351. doi: 10.1016/j.molstruc.2018.12.030
63. S.J.H.M.H.M. Jessima, A. Berisha, S.S.S.S. Srikandan and S. Subhashini, Preparation, characterization, and evaluation of corrosion inhibition efficiency of sodium lauryl sulfate modified chitosan for mild steel in the acid pickling process, *J. Mol. Liq*., 2020, **320**, 114382. doi: 10.1016/j.molliq.2020.114382
64. M. Rbaa, P. Dohare, A. Berisha, O. Dagdag, L. Lakhrissi, M. Galai, B. Lakhrissi, M. Ebn Touhami, I. Warad and A. Zarouk, New Epoxy sugar based glucose derivatives as eco friendly corrosion inhibitors for the carbon steel in 1.0 M HCl: Experimental and theoretical investigations, *J. Alloys Compd*., 2020, **833**, 154949. doi: 10.1016/j.jallcom.2020.154949
65. R. Hsissou, O. Dagdag, S. Abbout, F. Benhiba, M. Berradi, M. El Bouchti, A. Berisha, N. Najjaji and A. Elharfi, Novel derivative epoxy resin TGETET as a corrosion inhibition of E24 carbon steel in 1.0 M HCl solution. Experimental and computational (DFT and MD simulations) methods, *J. Mol. Liq*., 2019, **284**182–192. doi: 10.1016/j.molliq.2019.03.180.
66. O. Dagdag, A. Berisha, Z. Safi, S. Dagdag, M. Berrani, S. Jodeh, C. Verma, E.E. Ebenso, N. Wazzan and A. El Harfi, Highly durable macromolecular epoxy resin as anticorrosive coating material for carbon steel in 3% NaCl: Computational supported experimental studies, *J. Appl. Polym. Sci*., 2020, **137**, no. 34, 49003. doi: 10.1002/app.49003.
67. M. Damej, R. Hsissou, Avni Berisha, K. Azgaou, M. Sadiku, M. Benmessaoud, N. Labjar and S. El hajjaji, New epoxy resin as a corrosion inhibitor for the protection of carbon steel C38 in 1M HCl. Experimental and theoretical studies (DFT, MC, and MD), *J. Mol. Struct*., 2022, **1254**, 132425. doi: 10.1016/j.molstruc.2022.132425
68. V.V. Mehmeti and A.R. Berisha, Corrosion study of mild steel in aqueous sulfuric acid solution using 4-methyl-4H-1,2,4-triazole-3-thiol and 2-mercaptonicotinic acid – an experimental and theoretical study, *Front. Chem*., 2017. doi: 10.3389/fchem.2017.00061
69. M. Damej, A. Molhi, K. Tassaoui, B. El Ibrahimi, Z. Akounach, A. Ait Addi, S. El hajjaji and M. Benmessaoud, Experimental and Theoretical Study to Understand the Adsorption Process of p-Anisidine and 4-Nitroaniline for the Dissolution of C38 Carbon Steel in 1M HCl, *ChemistrySelect*, 2022, **7**, no. 2, e202103192. doi: 10.1002/slct.202103192

♦ ♦ ♦